Investigation on solid-liquid flow in the rear chamber of multi-stage slurry pumps with leakage flow

Bo Hu, Friedrich-Karl Benra, Weigang Lu, Hans Josef Dohmen

Investigation on solid-liquid flow in the rear chamber of multi-stage slurry pumps with leakage flow

Bo Hu[1]*, Friedrich-Karl Benra[2], Weigang Lu[3], Hans Josef Dohmen[4]

ISROMAC 2016
International Symposium on Transport Phenomena and Dynamics of Rotating Machinery
Hawaii, Honolulu
April 10-15, 2016

Abstract

Submersible multi-stage slurry pumps are widely used in mining industry. A sand discharge groove is designed to accomplish sand exclusion. The leakage flow through the broken balance hub is common in this kind of pumps. Whether the sand discharge groove will work when there is leakage flow is very important. The commercial RANS solver Ansys CFX 14.0 is used to predict the cavity flow in the rear chamber. The influences of leakage flow on the cavity flow are analyzed in this paper. The sand discharge capacities of the groove with and without leakage flow are also compared with each other. The simulation results show that most of the sand is discharged out of the rear chamber even if there is leakage flow. The results from the abrasion tests indicate that the simulation results are reasonable. The sand discharge groove will work even if there is leakage flow. The service life of the pump is dramatically improved.

Keywords

Solid-liquid flow—multi-stage slurry pump —leakage flow —abrasion test

[1,2,4] *Department of Mechanical Engineering, University of Duisburg-Essen, Duisburg, Germany*
[3] *China national research center of pumps, University of Jiangsu, Zhenjiang, China*

***Corresponding author:** bo.hu.1987@stud.uni-due.de*

NOMENCLATURE

A	axial coordinate
Ats	accumulated time step
b	radius of the disk
F_a	axial thrust
G	dimensionless gap width
H	pressure head
n	speed of rotation
N_{lg}	grid number of the leakage gap
p_0	pressure at pump outlet when t=0
p_t	pressure at pump outlet when t=t
p_{r1}	ratio of value of pressure at monitor point 1 to that when N_{lg}=0.29 million
p^*	pressure ratio of p_t to p_0
Q	volume flow rate
q	leakage volume flow rate
Δr	dimensionless radial gap
r	dimensionless radial coordinate
R	radial coordinate
R_i	radial coordinate of monitor points
Re_φ	circumferential Reynolds Number
ΔR	radial gap
s	axial gap
$SMSP$	submersible multi-stage slurry pump
t	time
T	total time
v_r	dimensionless radial velocity
v_θ	dimensionless tangential velocity
z	dimensionless axial gap
η	pump efficiency
φ_s	solid volume fraction
Ω	angular speed of the disk

INTRODUCTION

Flow in rotating cavity is an interesting issue. Batchelor[1] noticed the presence of both the disk layer and wall layer, which are separated by a central core of fluid. Daily and Nece[3] distinguished four different flow regimes based on the circumferential Reynolds Number Re_φ and the dimensionless gap width G. Djaoui et al. [5] investigated the influence of peripheral conditions on the flow pattern in an open cavity without superimposed flow. Kurokawa et al.[7] put forward the three-layer model for flow Regime IV, which is widely used in the industry. Will et al. [10,11] investigated the flow in the side chambers of a centrifugal pump. Poncet et al.[8] put forward a equation to calculate the values of core rotation factor, noted as β. β is the ratio of the angular velocity of fluid in the central core to that of disk. With centripetal inflow，expressed as follows:

$$\beta=2\times(5.9\times\frac{qRe_\varphi{}^{0.2}}{2\pi\Omega R^3}+0.63)^{5/7}\text{-}1 \qquad (1)$$

Bo Hu et al. [2] investigated the solid-liquid flow in the rear chamber of a submersible multi-stage slurry pump, noted as *SMSP*. A sand discharge groove is designed to accomplish sand exclusion，shown in Figure 1(a). It includes two parts: an annular groove at the outer radius of stator and a spiral groove on the inner surface of the stator. The diameter and the lead of the spiral groove are 5 mm and 85 mm, respectively. The diameter of the annular groove is also 5 mm. There are four sand discharge grooves in circumferential direction. From the results of former studies[2,10], the micro-sized sand, whose maximum length does not exceed 0.1 mm, moves with the conveying fluid. The flow regime in the cavity is still Regime IV, even if the flow contains the micro-sized sand. A central core separates the disk layer and the wall layer. Due to mass conservation, an axial convection of fluid from the outer radius of the disk to that of stator takes place. Although the cavity is open and the disk is not infinite, effective sand exclusion can be accomplished based on the axial convection and the three-layer model, shown in Figure 1(b).

The geometries of the rear chamber with sand discharge groove are shown in the Figure 2. The sand discharge groove, however, is designed assuming that there is no leakage flow. In mining applications, however, the *SMSPs* start to work when there is some sand to discharge. In the rest of the time, they are switched off. Since there is large pressure difference between the rear chamber and the environment, the O-ring marked in Figure 2 is fragile. From abrasion test, when the p^*, the ratio of p_t to p_0, drops by 10%, the O-ring is broken. It is quite hard to find whether the O-ring in the mechanical seal is broken before a pump starts to work. Sometimes, the *SMSP* has to work with a broken O-ring. The leakage flow is shown in Figure 2. From Eq. (1), the values of β increase with the increase of leakage flow rate, noted as q. With larger tangential velocities, the micro-sized is more likely to move radial outwards. After that, the sand may enter the annular grooves and be discharged along the spiral grooves. This paper presents the flow in the rear chamber of a *SMSP* with (after the O-ring is broken) and without leakage flow (before the O-ring is broken) when the *SMSP* is started.

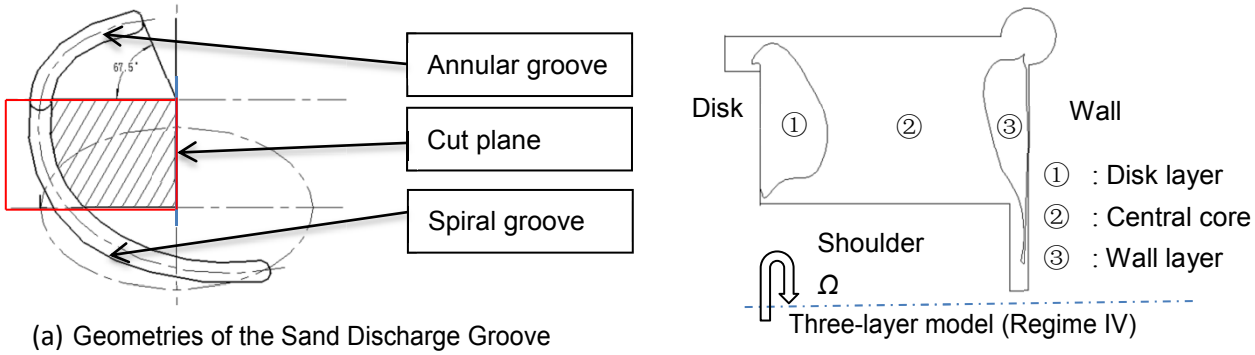

(a) Geometries of the Sand Discharge Groove

Figure 1. Sand Dischage Groove and Flow Regime in the Rear Chamber

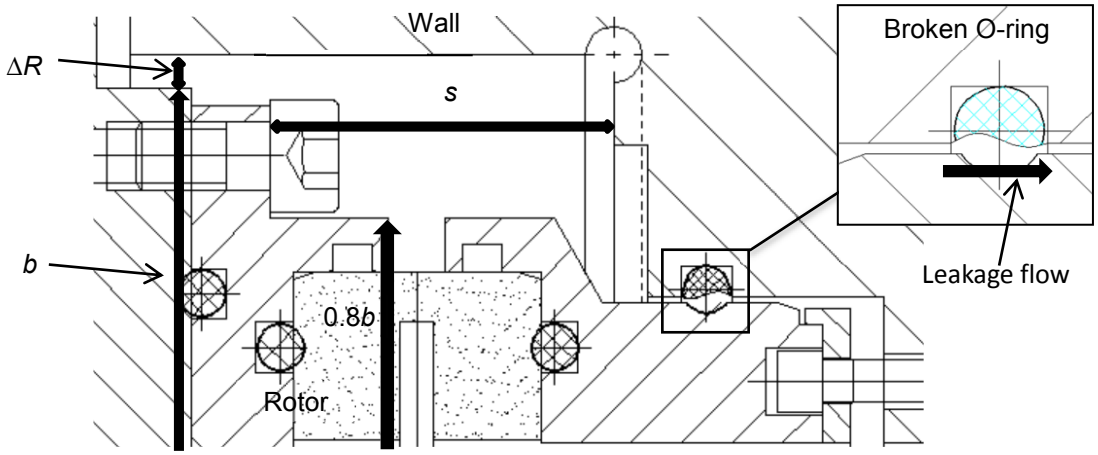

Figure 2. Sand Discharge Groove in the Rear Chamber and Leakage Flow

1. NUMERICAL SIMULATION

The numerical analyses on the last stage of the *SMSP* are carried out with the commercial ANSYS CFX 14.0 code. From Figure 3, the flow domains include five parts: inlet, impeller, cavity with rear chamber, leakage gap, and the volute with two outlets. The height of leakage gap is measured during the abrasion test (when p^* drops by 10%). The meshes are also shown in the Figure 3. The cavity with both rear chamber and spiral groove are generated with hybrid grids. The rest of domains are meshed with structured grids.

The analysis type is set as transient. This study focuses on the concentration of sand in the rear chamber. If the total time is too short, the concentration of sand may not change dramatically. To shorten the simulation period, the time step should not be too small. In this study, the time duration is set as total time t=3 s. and the time step is set as 0.05 s. The transient scheme is set as second order backward Euler to improve simulation precision. Standard k-ε model is used to predict the turbulent flow. The movements of dispersed phase (sand) are predicted based on the Euler-Euler approach. All the particles in the cavities are considered to have a spherical shape. The diameters of the particles are set as 0.1 mm. The granular temperature model is set as zero equation. Schiller-Naumann drag model[13] is used to calculate the drag force. The lift force of particles is calculated with Saffman-Mei lift force model[14]. Both turbulent dispersion force and wall lubrication force between particles and wall are ignored during the simulation. Instead of resolving boundary layers, scalable wall functions are used to model the viscous effects in the near wall regions. The basic idea behind the scalable wall-function approach is to limit the value of y*, which is used in the logarithmic formulation by the value of y^+=max (y*, 11.06). 11.06 is the intersection between the logarithmic and the linear near wall profile. All the mesh points are outside the viscous sub-layer and all fine mesh inconsistencies are avoided. The temperature of slurry is set as 20 ^oC. Since the volute has two outlets, the flow rates through the two outlets are considered as an equal value. Based on the design requirements, the values of mass flow rate at inlet, pressure at outlet and solid volume fraction are set as 5.4 kg/s, 2.6 MPa and 10%, respectively. The leakage flow rate is set as according to the results from abrasion test, obtained by a turbine flow meter (about 0.139 kg/s). The surface roughness value of all the domains is 12.5 μm. The speed of rotation interface between rotatable parts and liquid is 2900/min.

The locations of monitor points are shown in Figure 4. Their positions are given in Table 1. Monitor point 1, 2 and 3 are close to the disk and the rest of the monitor points are near the wall. The dimensionless axial coordinate z and the dimensionless radial coordinate r are defined as:

$$z = \frac{A}{s},\ r = \frac{R}{b} \tag{2}$$

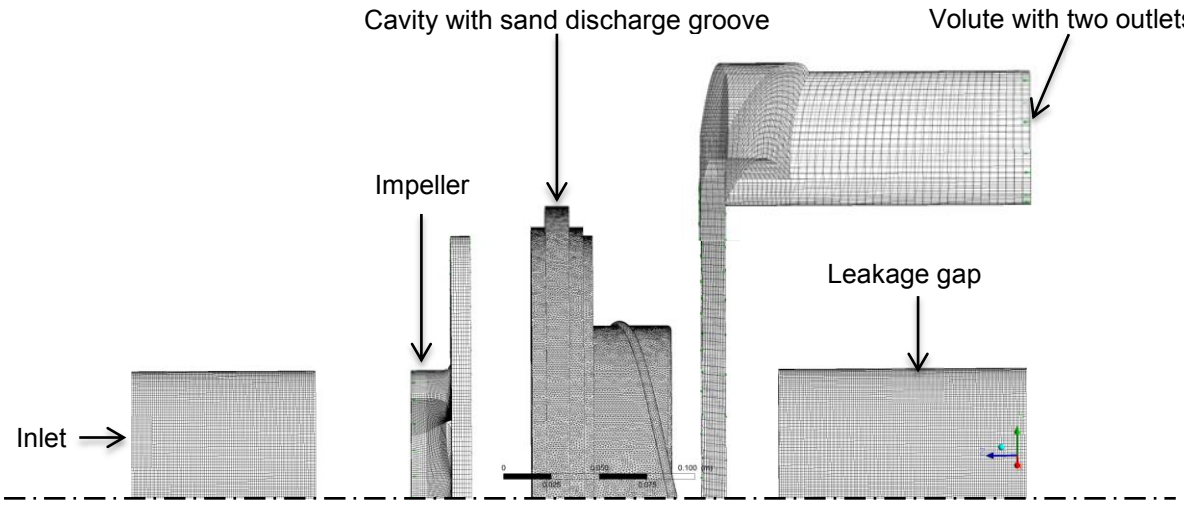

Figure 3. Domains and Meshes of Simulation Model

Table 1. Position of Monitor Points

	Point 1	Point 2	Point 3	Point 4	Point 5	Point 6
z	0.1	0.1	0.1	0.9	0.9	0.9
r	0.88	0.92	0.96	0.88	0.92	0.96

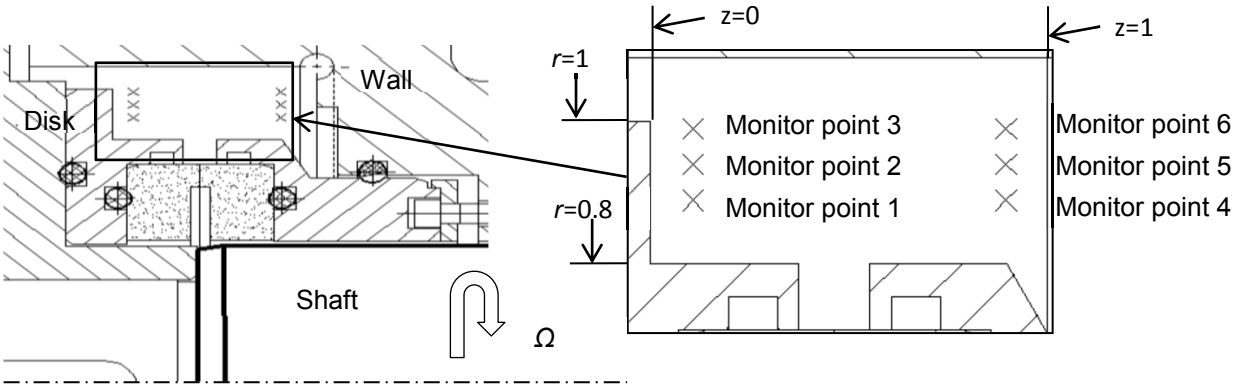

Figure 4. Arrangement of Monitor Points in the Rear Chamber

The residual type is *RMS* and the convergence criteria of transient simulation are set as 10^{-4}. In former studies[2], the mesh independence studies for impeller and volute have been accomplished. Hence, only the leakage gap is meshed with different grid numbers to perform mesh sensitivity analyses. The grid numbers of the rest of domains do not change. The total grid number of the leakage gap is noted as N_{lg}. p_{r1} is the ratio of value of pressure at monitor point 1 to that when N_{lg}=0.29 million. According to the results in Figure 5, the fine grid number of the leakage gap is 0.2 million.

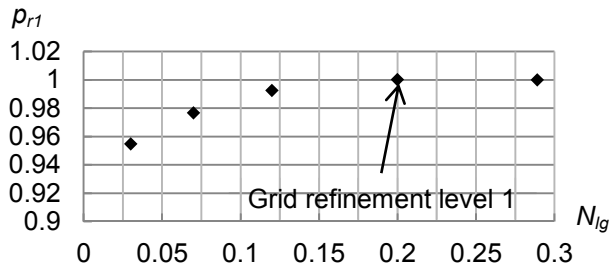

Figure 5: Mesh Sensitivity Analysis

The history of scaled residuals of simulation with leakage flow is given in Figure 6. The residuals without leakage flow are similar. The analyses are considered to be converged. During the simulation, the values of pressure, both radial and tangential velocity at the monitor points are monitored.

2. RESULTS AND DISCUSION

In this section, experimental data and simulation results are presented in order to analyze the sand discharge capacity. All the velocities are made dimensionless by dividing $\Omega \cdot b$.

2.1 Movements of particles

In this study, only the movements of sand and contours on the cut plane, pointed out in Figure 1(a), are shown. The annular groove and the spiral groove are connected on this surface. If the sand is predicted in the groove on that surface, it is more likely to be discharged along the spiral groove.

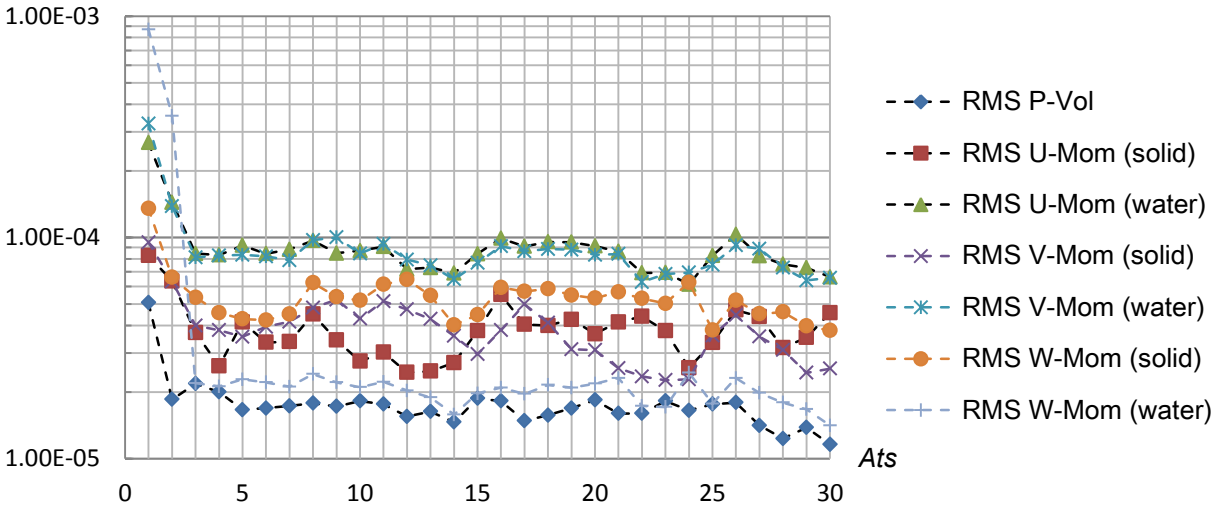

Figure 6. Convergence Behavior of Simulation with Leakage Flow

When t=3 s, the movements of particles on the meridian plane (the cut plane pointed out in Figure 1(a)) are predicted to analyze the influence of leakage flow on the sand discharge capacity, shown in Figure 7. The directions of arrows show the movements of particles. When the sand enters the leakage gap, it may rotate and remain inside when there is no leakage flow. A lot of sand enters the groove in the rear chamber with or without leakage flow. With large tangential velocity, the sand may be discharged along the spiral groove when enters the sand discharge groove. The leakage flow does not have large influence on the cavity flow. It seems that the sand discharge groove will work even if there is leakage flow.

2.2 Distribution of v_r

The variations of v_r at the first three seconds are shown in Figure 8. The positive and negative values represent radial outward flow and radial inward flow, respectively. The values of v_r vary relative more widely near the disk (point 1 to point 3) than near the wall. The values of v_r near the disk are slightly smaller in general when leakage flow occurs, as indicated in Figure 7(a). The radial inward superimposed flow decreases the values of v_r near the rotor. Near the wall (point 4 to point 6), the fluid moves towards the shaft with relative higher values of v_r when leakage occurs. The reason is that part of the flow moves towards the shaft and then flow through the leakage gap.

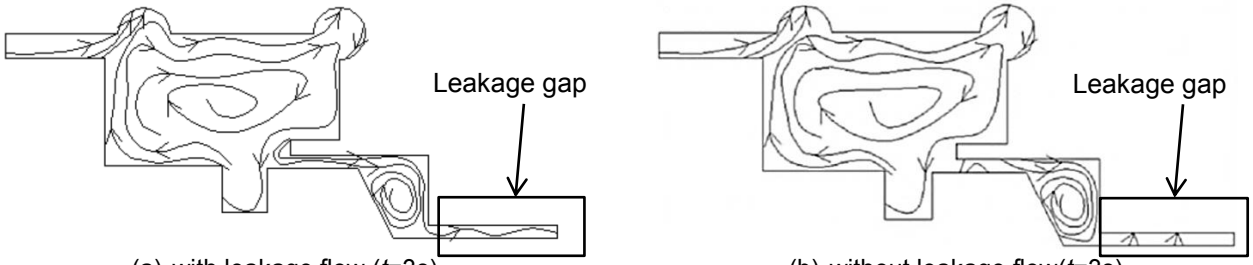

(a) with leakage flow (t=3s) (b) without leakage flow(t=3s)

Figure 7. Movements of Particles

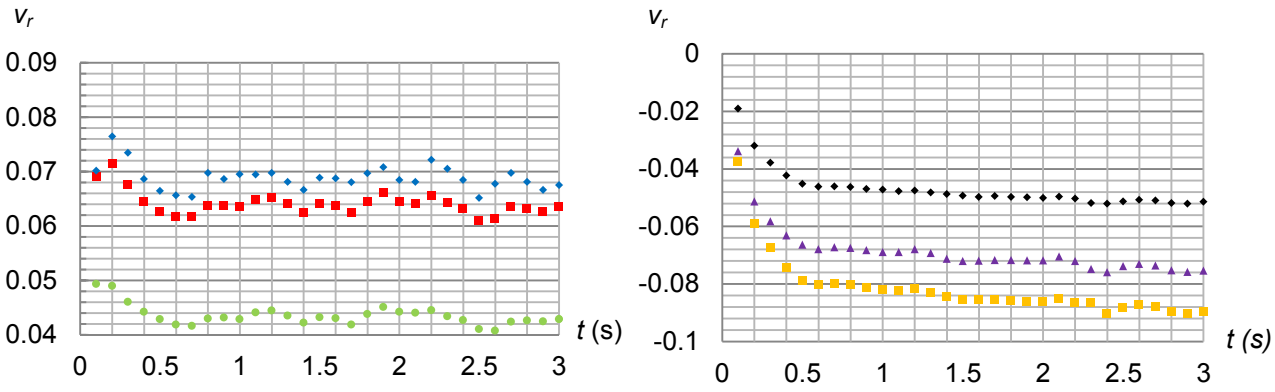

(a) With leakage flow

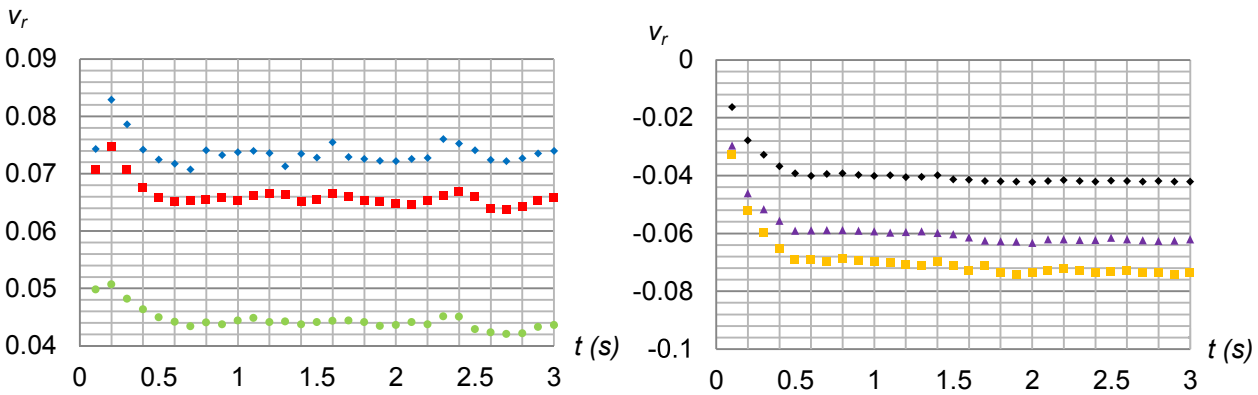

(b) Without leakage flow

◆ Point 1 ■ Point 2 ● Point 3 ◆ Point 4 ▲ Point 5 ■ Point 6

Figure 8. Variation of the Radial Velocity with Leakage Flow

2.3 Distribution of v_θ

The simulation results of dimensionless tangential velocity, noted as v_θ, at the first three seconds, are shown in Figure 9. The values of v_θ vary more widely near the wall than the near the disk. The values of v_θ in the cavity with leakage flow are slightly higher than those without leakage flow in general. The reason is that the radial inward superimposed flow will push the fluid, which has larger values of tangential velocity, radial inwards. With large tangential velocity, the micro-sized sand in the disk layer and the central core is more likely to move radial outwards and then enter the sand discharge groove. The results indicate that the sand discharge capacity may be better when leakage flow occurs.

2.4 Prediction of the sand discharge capacity

The distributions of solid volume fraction, noted as φ_s, at the first three seconds without leakage flow are shown in the Figure 10. The value of φ_s at pump inlet remains 10%. The values of solid volume fraction drop obviously in three seconds. The highest solid volume fractions occur both in the sand discharge groove and in the leakage gap. The concentrations of sand in the leakage flow near the wall are also high. The high concentration of sand in the leakage gap indicates that the sand is hard to be discharged out of the leakage gap when there is no leakage flow.

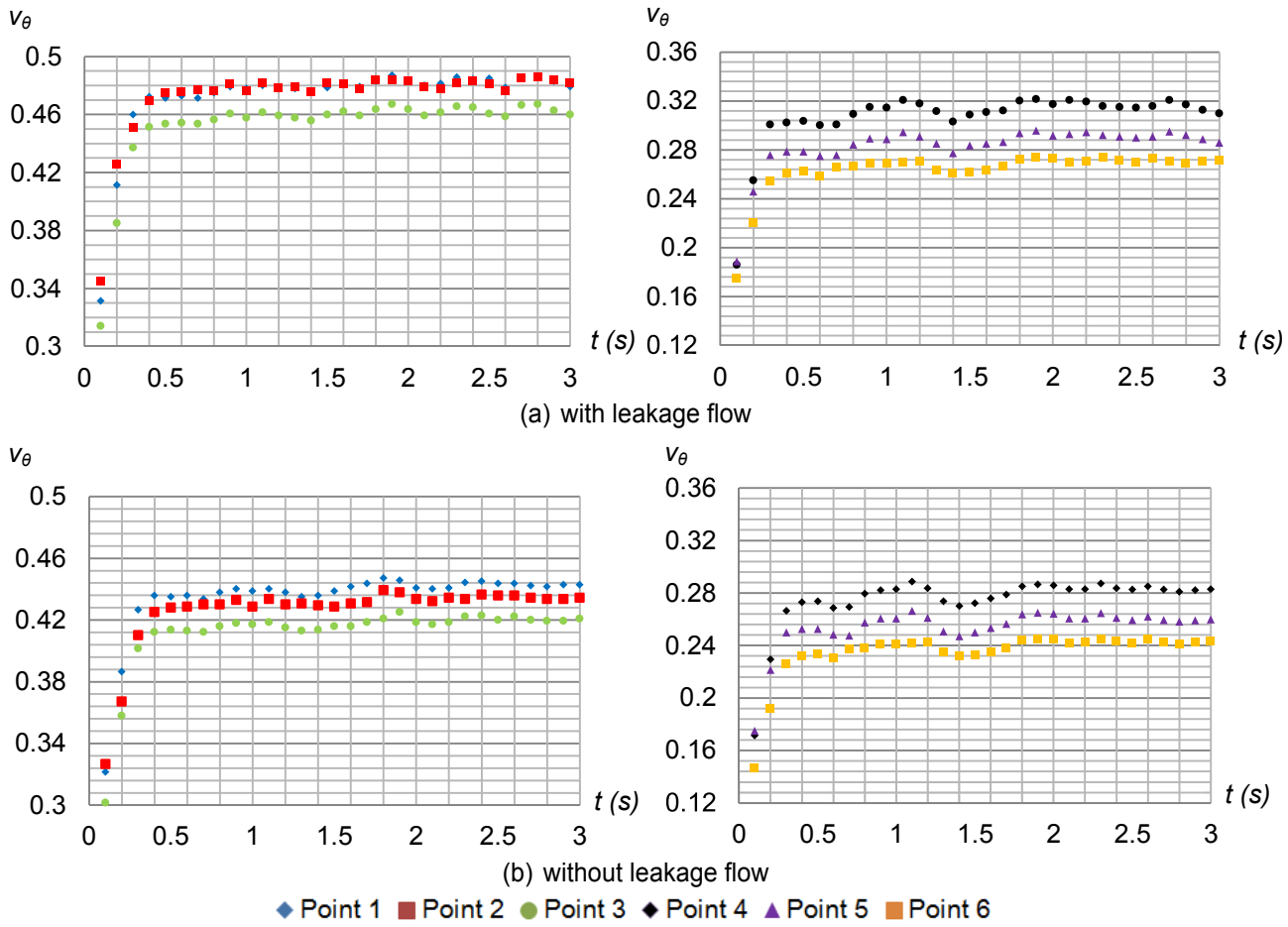

Figure 9. Variation of the Tangential Velocity with Leakage Flow

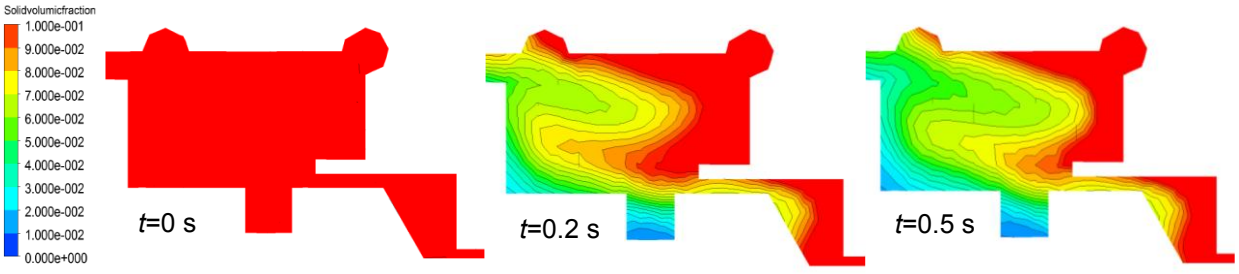

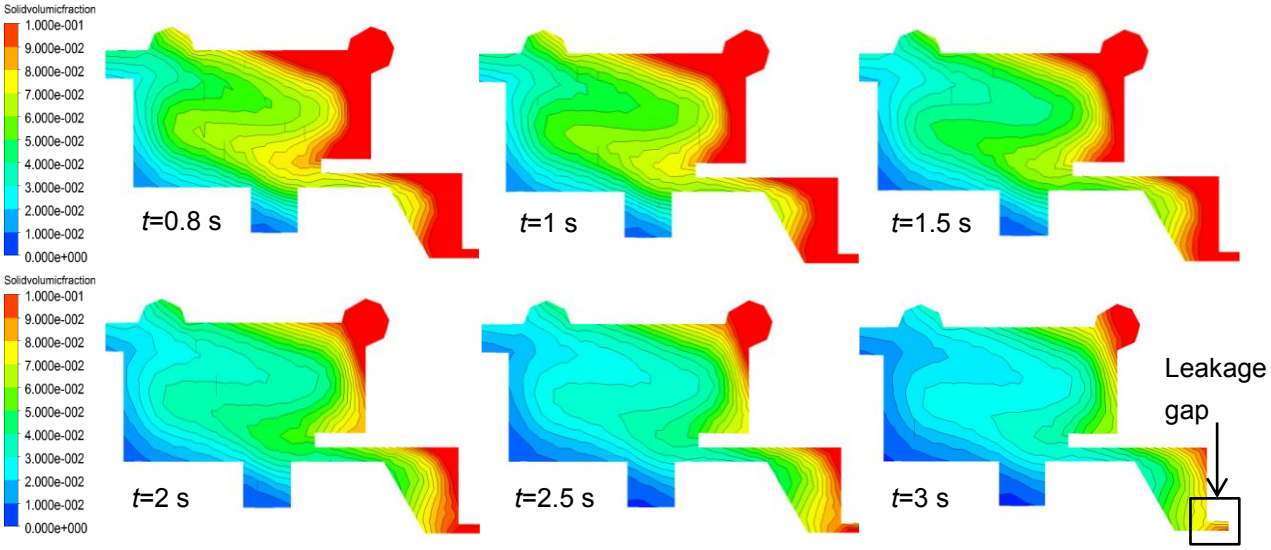

Figure 10. Variation of the Solid Volume Fraction without Leakage Flow

The distributions of φ_s at the first three seconds when leakage flow occurs are shown in Figure 11. The value of φ_s at pump inlet remains 10%. The highest solid volume fractions are shown in the spiral groove. When the *SMSP* with broken O-ring starts (t=0), the leakage flow contains high concentration of sand (φ_s=10%). The values of particle concentration on the cut plane drop to lower values than those without leakage flow in three seconds. The sand discharge capacity of groove is better in the cavity with leakage flow. The simulation results also indicate that when the sand is discharged out of the rear chamber, it is hard for them to enter the rear chamber again. That may be the reason why the φ_s in the groove is lower after t=2 s.

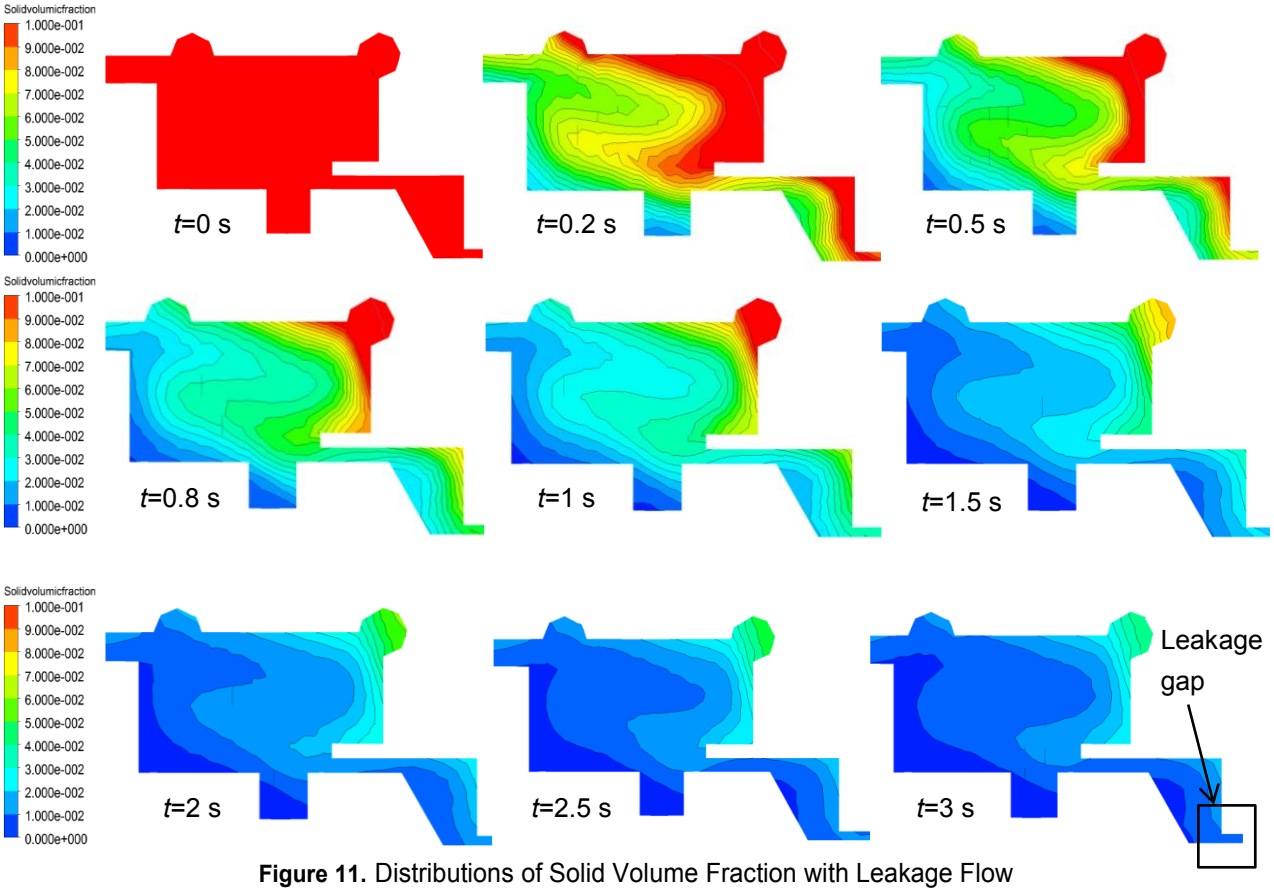

Figure 11. Distributions of Solid Volume Fraction with Leakage Flow

The variations of φ_s in the leakage flow are shown in the Figure 12. When leakage flow occurs, the value of φ_s in the leakage flow is higher than the value of φ_s (10%) when t=0 s. The values of φ_s plunge in three second from around 20% to around 2%. This indicates that most of the sand is discharged out of the rear chamber. The sand discharge capacity of groove is better when there is leakage flow. Since the concentration of sand in the leakage flow drops, the service life of mechanical seal may be improved.

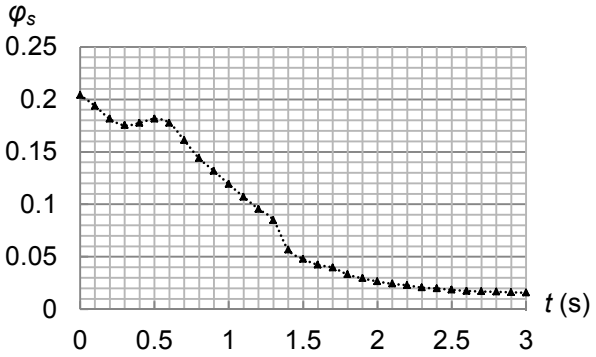

Figure 12. Variation of Solid Volume Fraction in the Leakage Flow

2.5 Axial thrust analysis

The variations of the axial thrust of the last stage, noted as F_a, are shown in the Figure 13. Since the axial thrust of the 6-stages pump is large, the axial thrust should be carefully analyzed to make sure that the bearing system is safe when leakage flow occurs. The values of axial thrust of the last stage vary greatly from t=0 s to t=3 s. When leakage flow occurs, the values of axial thrust are much smaller, which indicate that the load on the bearing will decrease and the service life of the bearing may be longer.

3. TEST RESULTS

The results from abrasion test are provided in this part in order to verify the correctness of simulation results. The test rig meets the requirements of international B-grade precision (ISO9906-1999) [2]. A pressure transmitter with the uncertainty of 0.1% measures the pressure at pump outlet to calculate the pressure head, noted as H. The flow of the pump is measured by a turbine flow meter with the uncertainty of 0.2%. The density of the slurry is 1160 kg/m^3. The temperature of the slurry is 20℃. This test rig has circulation system at the bottom to reduce the settlement of sand. The size of the sand is selected with a screen mesh. During the test, the concentration of sand is measured every 48 hours. Appropriate sand is added to the slurry when the sand concentration decreases by more than 20%.
The values of outlet pressure are recorded during the test. When the O-ring is broken, large pressure difference contributes to large leakage flow from the rear chamber (approximate 2 MPa) to the environment. It results in the plunge of pressure head, shown in Figure 14.
One of the SMSP is produced with sand discharge groove. The other is used for comparison. When p^* drops by 10%, the mechanical seal is considered to fail because the O-ring is broken. Two pumps are switched off and the geometries of the mechanical seal are measured. When the pumps are restarted, there are leakage flows in both of the pumps. The decrease rate of the p^* in the *SMSP* with sand discharge groove is less than that without sand discharge grove. The results show that the sand discharge groove will work even if there is leakage flow.

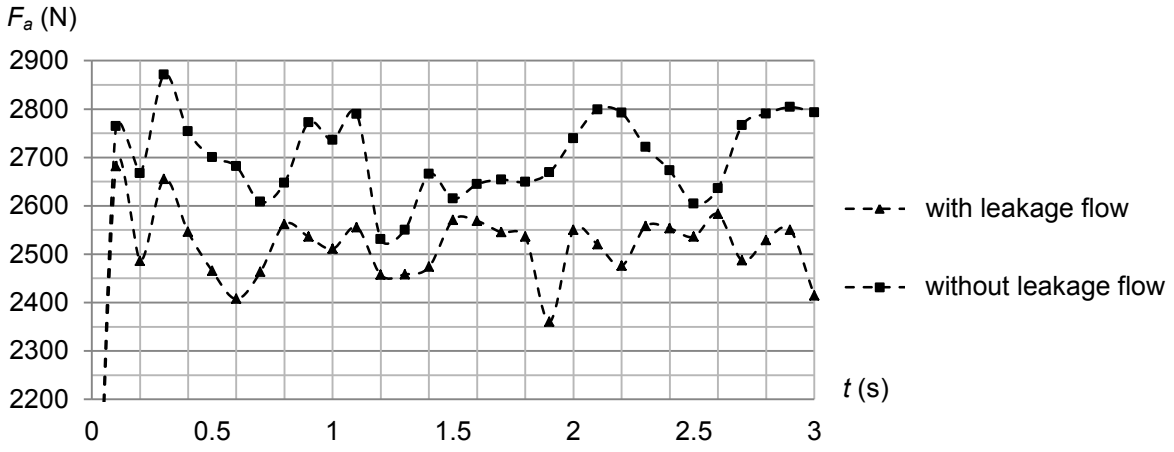

Figure 13. Variations of the Axial Thrust of the Last Stage

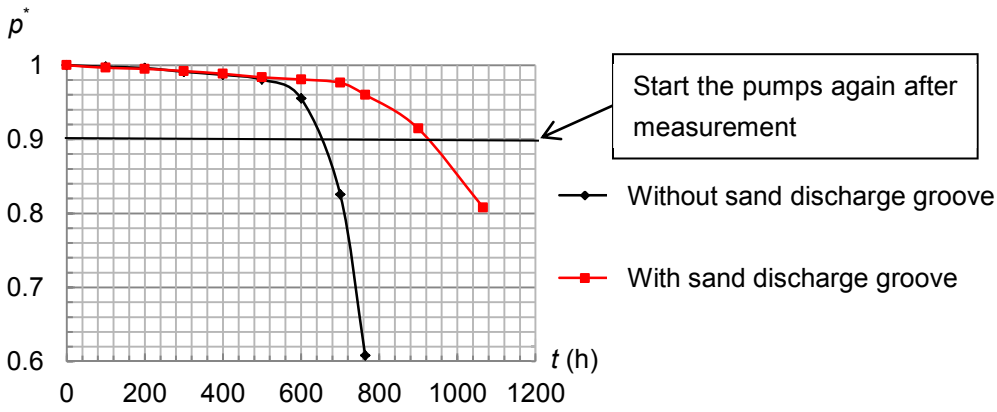

Figure 14. Results of Abrasion Tests

4. CONCLUSION

The sand discharge groove, designed based on Batchelor type flow, will work even if there is leakage flow.

From Poncet's equation, the leakage flow will results in greater value of β. Associated with the simulation results, the leakage flow contributes to larger tangential velocity in the central core and near the disk. The sand is more likely to move radial outward and enter the groove. The sand discharge capacity of the groove may be better when there is leakage flow.

The abrasion test shows that the simulation results are reasonable and the service life of *SMSP* is dramatically improved.

ACKNOWLEDGEMENTS

This study is funded by CSC (China Scholarship Council).

REFERENCES

[1] Batchelor, G. K. Note on a class of solutions of the Navier-Stokes equations representing steady rotationally-symmetric flow. The Quarterly Journal of Mechanics and Applied Mathematics, Vol. 4, No. 1, 29-41，1951.

[2] Bo Hu, Benra, F.-K., Weigang Lu. Investigation on the solid-liquid flow in the rear chamber of a submersible multi-stage slurry pump. 11th European Conference on Turbomachinery Fluid Dynamics and Thermodynamics, Madrid, Spain, 2015.

[3] Daily, J. W., Nece, R. E. Chamber dimension effects on induced flow and frictional resistance of enclosed rotating disks. Journal of Basic Engineering, 82:217-232, 1960.

[4] Debuchy, R., Poncet, S., Abdel Nour, F., Bois, G. Experimental and numerical investigation of turbulent air flow behavior in a rotor-stator cavity. 8th European Turbomachinery Conference, Graz, Austria, 2009.

[5] Djaoui, M., Malesys, A., Debuchy, R. Mise en evidence expérimentale de la sensibilité de l'écoulement de type rotorstator aux effets de bord. C. Acad. Sci. Paris. t. 327, Série II b, 49-54, 1998.

[6] Emmanuel D'Haudt, Stefania Della Gatta, Roger Debuchy, Gerard Bois, Francesco Martelli. Assessment of experimental and numerical flow investigation in rotating-disc systems. The Eleventh International Symposium on Transport Phenomena and Dynamics of Rotating Machinery, Honolulu, Hawaii, USA, 2006.

[7] Kurokawa, J., Sakuma, M. Flow in a narrow gap along an enclosed rotating disk with through-flow. JSME International Journal, Series II, Vol. 31, No.2, 243-251, 1988.

[8] Poncet, S., Chauve, M. P., and Le Gal, P. Turbulent Rotating Disk Flow With Inward Throughflow, Journal of Fluid Mechanics. 522, pp. 253–262, 2005.

[9] Randriamampianina, A., Elena, L., Fontaine, J. P., Schiestel, R. Numerical prediction of laminar. transitional and turbulent flows in shrouded rotor-stator systems, Phys. Fluids, 9, 1696-1712, 1997.

[10] S. B. Hazra, K. Steiner. Computation of dilute two-phase flow in a pump. Journal of Computational and Applied Mathematics, 203, 444–460, 2007.

[11] Will, B. C., Benra, F.-K., Dohmen, H. J. Numerical and experimental investigation of the flow in the side cavities of a centrifugal pump. The 12th International Symposium on Transport Phenomena and Dynamics of Rotating Machinery, ISROMAC13-2009-0002, Honolulu, Hawaii, USA, 2010.

[12] Will, B. C., Benra, F.-K., Dohmen, H. J. Investigation of the flow in the side chambers of a

centrifugal pump with volute casing. 10th International Symposium on Experimental Computational Aerothermodynamics of Internal Flows, Brussels, Belgium, 2011.

[13] Mohsen Karimi, Guven Akdogan, Kiran H. Dellimore, Steven M. Bradshaw. Comparison of different drag coefficient correlations in the CFD modelling of a laboratory-scale rushton-turbine flotation tank. 9th International Conference on CFD in the Minerals and Process Industries, CSIRO, Melbourne, Australia, 1-7, 2012.

[14] P. Cherukat, J.B. McLaughlin, D.S. Dandy. Guven Akdogan, Kiran H. Dellimore, Steven M. Bradshaw. A computational study of the inertial lift on a sphere in a linear shear flow field International Journal of Multiphase Flow, 1999.